Evidence that $\Delta S^{\ddagger}$ Controls Interfacial Electron Transfer Dynamics from Anatase TiO_2 to Molecular Acceptors

Ludovic Troian-Gautier, Brian N. DiMarco, Renato N. Sampaio, Seth L. Marquard, and Gerald J. Meyer*

Department of Chemistry, University of North Carolina at Chapel Hill, Chapel Hill, North Carolina, 27599, United States

Abstract

Recombination of electrons injected into TiO_2 with molecular acceptors present at the interface represent an important loss mechanism in dye-sensitized water oxidation and photochemical electrical power generation. Herein, the kinetics for this interfacial electron transfer reaction to oxidized triphenylamine (TPA) acceptors was quantified over a 70° temperature range for *para*-methyl-TPA (**Me**-TPA) dissolved in acetonitrile solution, 4-[N,N-di(*p*-tolyl)amino]benzylphosphonic acid (***a*-TPA**) anchored to the TiO_2 interface, and a TPA covalently bound to a ruthenium sensitizer, $[Ru(tpy\text{-}C_6H_4\text{-}PO_3H_2)(tpy\text{-}TPA)]^{2+}$ "**RuTPA**", where tpy is 2,2':6',2''-terpyridine. Activation energies extracted from an Arrhenius analysis were found to be 11 ± 1 kJ mol^{-1} for **Me**-TPA and 22 ± 1 kJ mol^{-1} for ***a*-TPA**, values that were insensitive to the identity of different sensitizers. Recombination to $\mathbf{RuTPA}^+$ proceeded with E_a = 27 ± 1 kJ mol^{-1} that decreased to 19 ± 1 kJ mol^{-1} when recombination occurred to an oxidized *para*-methoxy TPA (**MeO**-TPA) dissolved in CH_3CN. Eyring analysis revealed a smaller entropy of activation $|\Delta S^{\ddagger}|$ when the ***a*-TPA** was anchored to the surface or covalently linked to the sensitizer, compared to that when **Me**-TPA was dissolved in CH_3CN. In all cases, Eyring analysis provided large and negative $\Delta S^{\ddagger}$ values that point toward unfavorable entropic factors as the key contributor to the barrier that underlies the slow recombination kinetics that are generally observed at dye-sensitized TiO_2 interfaces.

Introduction

Excited-state electron injection into wide bandgap semiconductor nanocrystallites interconnected in a mesoporous thin film represents a crucial first step in dye-sensitized water oxidation and halide oxidation for solar fuel or electrical power generation.[1-10] Fortunately, excited-state injection is known to occur quantitatively and on ultrafast time scales under a wide variety of experimental conditions.[11] Most practical applications also require that the injected electrons be quantitatively transported through the mesoporous thin film to the external circuit by avoiding recombination with interfacial acceptors. In optimized dye sensitized solar cells operating at short circuit conditions, every injected electron is indeed collected in the external circuit within reasonable experimental error while at the power point condition there is evidence for some unwanted recombination.[12] The situation for dye-sensitized water oxidation is far less optimal, as slow water oxidation results in significant recombination, even when core-shell nanostructured materials are used to inhibit this unwanted chemistry.[13-18] A fundamental study designed to quantify the activation barriers for charge recombination under conditions that can be exploited for practical water oxidation is presented herein.

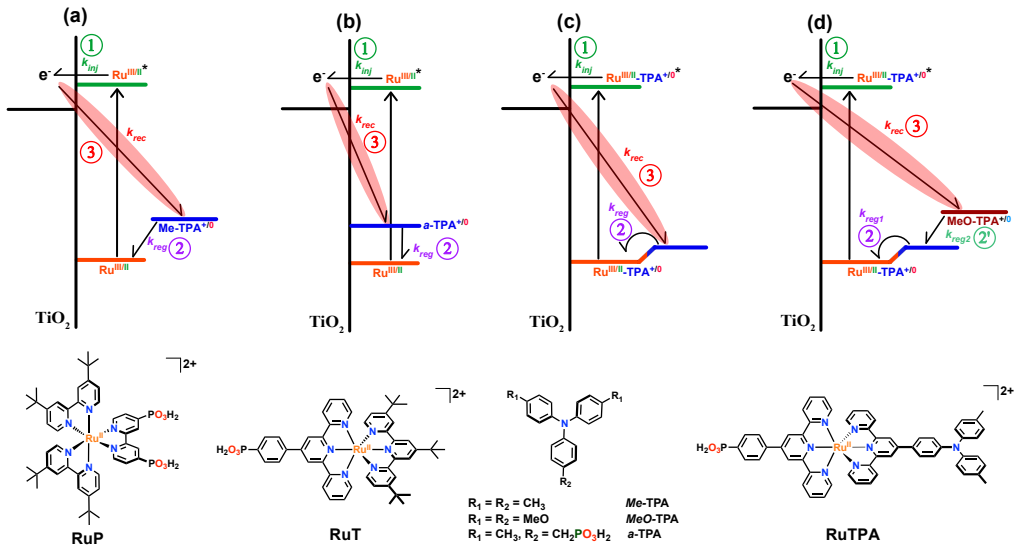

Figure 1. The TPA and Ru sensitizers utilized herein are shown as well as the four interfacial electron transfer reactions of injected electrons with oxidized triphenylamines. After visible light absorption, excited-state electron injection from the sensitizer to the acceptor state of TiO_2 occurs. In all cases, excited-state injection occurs (1) followed by regeneration with TPA (2) to yield an injected electron and an oxidized TPA that enabled the highlighted recombination reaction (3) to be quantified for TPA derivatives in fluid solution (a) and (d), anchored to TiO_2 (b), or covalently linked to the sensitizer (c). See text for more details.

This study utilizes triphenylamines (TPAs) that are either solvated in an acetonitrile solution (**Me**-TPA**, MeO**-TPA) that surrounds the mesoporous thin film, anchored to the TiO_2

surface (***a*-TPA**), or covalently linked to the dye sensitizer (**RuTPA**), **Figure 1**. The TPAs were chosen for their high stability in both their neutral and one electron oxidized forms, while also possessing a formal $E^o(TPA^{+/0})$ reduction potential that can be widely tuned.[19-20] These amines also absorb little visible light in their neutral state, in contrast to an intense absorption band in the red region upon oxidation. This feature makes them ideal for characterization by transient spectroscopic techniques. These spectroscopic and electrochemical properties of TPAs have also been exploited previously in a variety of solar cells.[21-23]

Reported herein is a systematic study of the unwanted recombination reaction between an injected electron and an oxidized TPA, represented by the highlighted red arrows (3) in **Figure 1**. Four different types of recombination reactions are reported, all of which are initiated by light absorption of a Ru polypyridyl sensitizer, followed by excited state electron injection (1), and electron transfer from TPA to the oxidized sensitizer (2). The physical location of the TPA was intentionally varied. Recombination to **Me**-TPA^+ occurred in fluid solution, **Figure 1a**, while **a-TPA**$^+$ was co-anchored with the sensitizer to the TiO_2 surface, **Figure 1b**. This reactivity was initiated with light absorption by two different sensitizers, a Ru-bipyridyl (**RuP**) or a Ru-terpyridyl (**RuT**) complex, which were found to behave very similarly. In the covalently linked **RuTPA**, excited-state injection by the ruthenium sensitizer was followed by intramolecular electron transfer from the pendant TPA group, **Figure 1c**, as well as a subsequent intermolecular electron transfer that enabled recombination to **MeO**-TPA^+ to be quantified, **Figure 1d**. Interestingly, the activation and kinetic parameters were distinctly different for these four interfacial electron transfer reactions; yet a very negative entropy of activation indicated that the unfavorable entropy change associated with localization of an injected electron on a single molecular acceptor contributes significantly to the large barrier and slow recombination that are generally found at dye-sensitized TiO_2 interfaces.

Results

The **RuP**, **RuT**, **RuTPA** and ***a*-TPA** compounds used in this study (**Figure 1**) were prepared and characterized by standard methods that are detailed in the Experimental Section. When dissolved in fluid acetonitrile solutions, **RuP** displayed a characteristic metal-to-ligand charge transfer (MLCT) band centered at 460 nm, while **RuT** and **RuTPA** exhibited more red-shifted MLCT features at 490 nm and 500 nm respectively. Shown in **Figure 2** are the visible absorption spectra of mesoporous TiO_2 thin films sensitized with **RuP**, **RuT** or **RuTPA** immersed in neat

CH_3CN or in 0.1 M $LiClO_4/CH_3CN$. When anchored to the TiO_2 surface, all ruthenium sensitizers retained their MLCT absorption band regardless of their surface coverage or the presence of a co-anchored TPA compound (see experimental section). The addition of 0.1 M $LiClO_4$ resulted in a bathochromic (red) shift of the MLCT band of **RuP**, consistent with prior observations made with similar Ru compounds (**Figure 2**).[24-26] The Li^+ induced spectral shifts were much less pronounced for **RuT**, and nearly indistinguishable for **RuTPA**. The neutral TPA derivatives showed an intense absorption band centered around 300 nm in CH_3CN with no appreciable absorption in the visible region.

Cyclic voltammetry measurements performed in 0.1M $LiClO_4/CH_3CN$ solutions showed reversible redox chemistry for all the TPAs used in this study (**Figure S2**). The formal reduction potentials $E°(TPA^{+/0})$ were estimated as the average potential between the anodic and cathodic peak currents, **Table 1**. Spectroelectrochemical measurements were performed to quantify the absorption spectrum of the one electron oxidized form of both the TPA and Ru(II) compounds. Upon oxidation, each TPA species displayed a strong absorption band centered between 670 nm and 720 nm, **Figure 2**. The oxidized **RuP** and **RuT** sensitizers displayed negligible absorption in the visible region. Regarding **RuTPA**, a simultaneous bleach of the MLCT concomitant with the appearance of the TPA^+ signal was observed upon oxidation (**Figure S3-S4**), as previously observed for similar compounds.[27] A summary of these spectral and electrochemical properties is presented in **Table 1**.

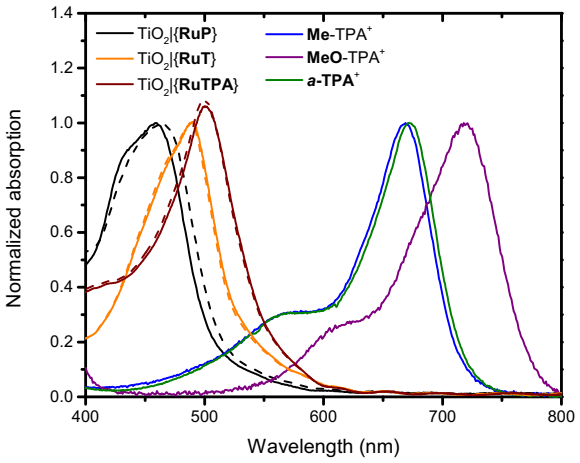

Figure 2. The visible absorption spectra of **RuP** (black)**, RuT** (orange) and **RuTPA** (brown) anchored to TiO_2 thin films immersed in CH_3CN (solid) or in 0.1 M $LiClO_4$ CH_3CN solution (dashed). The spectra of **Me-TPA**$^+$ (blue) ***a*-TPA**$^+$ (green) and **MeO**-TPA^+ (purple) in 0.1 M $LiClO_4$ CH_3CN solution are also given.

Table 1: Reduction Potentials and Absorption Maxima of the Ru Sensitizers and TPAs.[a]

	E^o (V vs NHE)	λ_{abs} (nm) (ε x10^4 M^{-1} cm^{-1})	λ_{abs} (nm) TPA^+ (ε x10^4 M^{-1} cm^{-1})
RuP	1.37	460 (1.4)	---
RuT	1.52	488 (2.1)	---
RuTPA	1.15; 1.67	502 (4.3)	670 (1.8)
***a*-TPA**	1.05	300 (2.5)a[b]	690 (2.4)[b]
***Me*-TPA**	0.99	301 (2.4)[c]	668 (2.4)[c]
MeO-TPA	0.72	296 (2.6)	717 (2.8)

[a] All data measured at room temperature in 0.1M $LiClO_4/CH_3CN$ solutions. [b]Values obtained from the ester derivative ***a*-TPA**. [c]Obtained from ref [20].

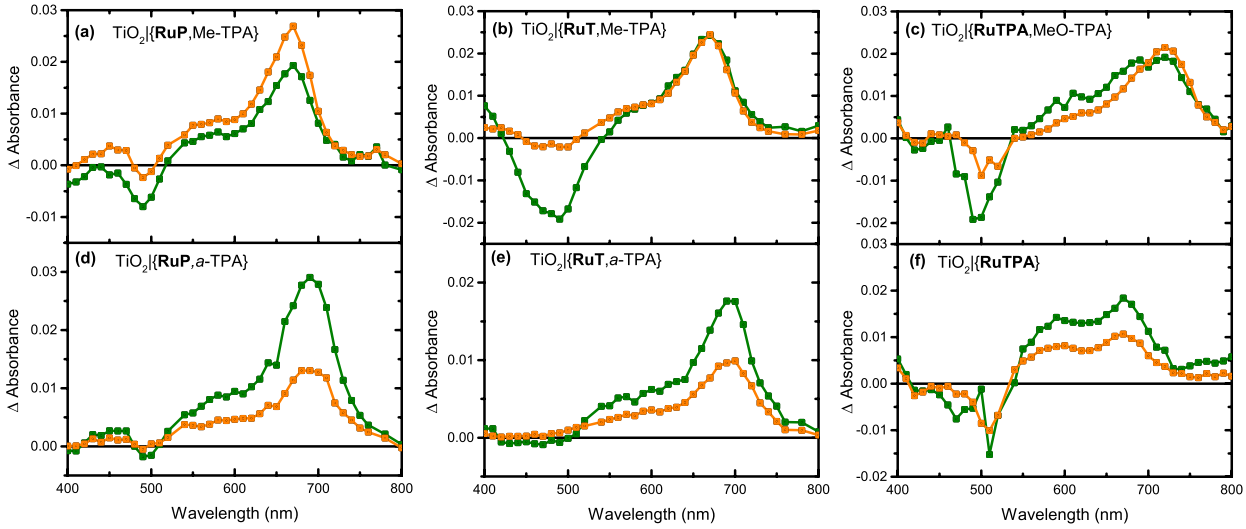

Figure 3. Absorption changes observed 50 ns (green) and 1 µs (orange) after pulsed 532 nm light irradiation of TiO_2|{**RuP**,**Me**-TPA} (a), TiO_2|{**RuT**,**Me**-TPA} (b), TiO_2|{**RuTPA**,**MeO**-TPA} (c), TiO_2|{**RuP**,***a*-TPA**} (d), TiO_2|{**RuT**,***a*-TPA**} (e) and TiO_2|{**RuTPA**} (f) submerged in argon saturated 0.1 M $LiClO_4$ CH_3CN electrolyte.

The transient absorption difference spectra generated after pulsed 532 nm laser excitation of mesoporous TiO_2 thin films sensitized with either **RuP** or **RuT** (abbreviated TiO_2|{**RuP**} or TiO_2|{**RuT**}) submerged in 0.1 M $LiClO_4/CH_3CN$ solution containing 30 mM Me-TPA are presented in **Figure 3a** and **b**. At early observation times (50 ns), spectral signatures assigned to the oxidized **Me**-TPA^+ as well as the oxidized sensitizer, $\mathbf{Ru^{III}P}$ or $\mathbf{Ru^{III}T}$ were observed. The concentration of the oxidized sensitizer decreased with the concomitant growth of **Me**-TPA^+, which

achieved a maximum after ~ 1µs. For TiO_2|{**RuP**}, an additional first derivative spectral signature was observed at ~500 nm attributed to a Stark effect.[24-26]

Single wavelength absorption changes were non-exponential and were adequately modeled using a single Kohlrausch-Williams-Watts (KWW) function given in **Equation 1**,

$$A(t) = A_0 e^{-(kt)^{\beta}} \quad (1)$$

where *k* represents a rate constant and ß, which ranges between 0 and 1, is inversely related to the width of a Lévy distribution.[28-29] An average rate constant was taken as the first moment with **Equation 2**, where Γ is the gamma function.

$$k_{kww} = \frac{k\beta}{\Gamma\left(\frac{1}{\beta}\right)} \quad (2)$$

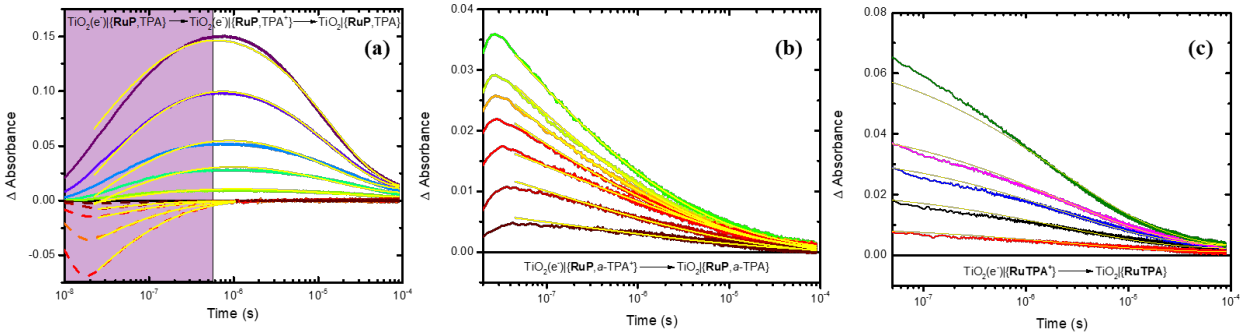

Figure 4. Absorption changes monitored at the TPA^+ maximum signal (positive signal) after pulsed 532 nm laser excitation of TiO_2|{**RuP**,**Me**-TPA} (a), TiO_2|{**RuP**,***a*-TPA**} (b) and TiO_2|{**RuTPA**} (c) in 0.1 M $LiClO_4$ CH_3CN electrolyte at various laser fluences. The purple region highlights the regeneration of $\mathbf{Ru^{III}P}$ by **Me**-TPA at 402 nm (negative signal) that is used to determine k_1 and β_1. Fits to the KWW model are overlaid on the data as solid yellow lines.

The transient absorption signatures of oxidized **Me**-TPA^+ monitored at 670 nm were biphasic as a result of diffusional regeneration (**Figure 4a**). A sum of two KWW functions adequately modeled the data. The loss of $\mathbf{Ru^{III}P}$ and $\mathbf{Ru^{III}T}$ was directly correlated with the appearance of **Me**-TPA^+ **(Figure 4a)**. The values for β and *k* obtained from the kinetic data for the reduction of $\mathbf{Ru^{III}P}$ and $\mathbf{Ru^{III}T}$ were fixed as β_1 and k_1 in the bi-KWW function used to model the **Me**-TPA^+ absorption changes. A value of $\beta_2 = 0.7$ was found to provide the best fits to the decay profile. An average rate constant, k_{kww}, of 5.8 ± 0.3 x10^4 s^{-1} and 8.2 ± 0.5 x10^4 s^{-1} for **RuP** and **RuT** respectively, were abstracted from these data using **Equation 2**. Excitation irradiance dependency studies resulted in normalizable absorption transients over a greater than ten-fold change in the initial concentration.

The absorption difference spectra generated after pulsed laser excitation of TiO_2 thin films cofunctionalized with a sensitizer (**RuP** or **RuT)** and ***a*-TPA** (TiO_2|{**RuP**,***a*-TPA**} and TiO_2|{**RuT**,***a*-TPA**}), are presented in **Figure 3d** and **e**. In contrast to the previous results where the TPA was present in the electrolyte, the ***a*-TPA** samples showed no absorption changes that could be attributed to $\mathbf{Ru^{III}}$ within the response time of our instrument (~20 ns), consistent with sub nanosecond regeneration of $\mathbf{Ru^{III}}$ to $\mathbf{Ru^{II}}$. Transient data corresponding to recombination with ***a*-TPA**$^+$ were modeled by a single KWW function, with $\beta = 0.17$ providing the best fits (**Figure 4**). Excitation irradiance data (**figure 4b**) were non-normalizable and displayed faster recombination rates with increasing initial concentrations. Representative data for TiO_2|{**RuT**,**Me**-TPA} and TiO_2|{**RuT**,***a*-TPA**} are gathered in the S.I (**Figure S5**)

Pulsed laser excitation of the covalently linked ruthenium-TPA (TiO_2|{**RuTPA**}) resulted in an instrument response limited appearance of **RuTPA**$^+$, $k_{obs} > 10^8$ s^{-1}, (**Figure 3f** and **Figure 4c**) whose spectral signature was in good agreement with that expected from spectroelectrochemical data. The average first-order rate constant for charge recombination was 1.3 ± 0.1 x10^5 s^{-1} with $\beta = 0.4$. Upon the addition of 20 mM **MeO**-TPA to the external solution (**Figure 3c**), the **RuTPA**$^+$ was rapidly (~100 ns) regenerated, with the appearance of **MeO**-TPA$^+$ (λ_{max} = 720 nm). Recombination of electrons in TiO_2 to **MeO**-TPA$^+$ were modeled using $\beta = 0.6$ for TiO_2|{**RuTPA**,**MeO**-TPA$^+$} that gave rise to an average rate constant of 6.9 ± 0.4 x10^4 s^{-1}. Note that this recombination process occurred at longer timescale than those observed for **Me**-TPA in solution.

The different recombination reactions between electrons in TiO_2 and **TPA**$^+$ acceptors described previously were monitored over a 70-degree temperature range (**Figure 5**). Representative data for TiO_2|{**RuP**,**Me**-TPA}, TiO_2|{**RuP**,***a*-TPA**} TiO_2|{**RuTPA**} and TiO_2|{**RuTPA**,**MeO**-TPA} are shown in **Figure 5** and the corresponding data for TiO_2|{**RuT**,**Me**-TPA} and TiO_2|{**RuT**,***a*-TPA**}, are gathered in the S.I (**Figure S6**). The extracted average rate constants, k_{kww}, were used to generate an Arrhenius plot (**Figure 6** and **Equation 3)**, from which activation energies were obtained, **Table 2**. Furthermore, Eyring analysis (**Figure 6** and **Equation 4**), revealed the enthalpies ($\Delta H^{\ddagger}$) and entropies ($\Delta S^{\ddagger}$) of activation that are summarized in **Table 3**.

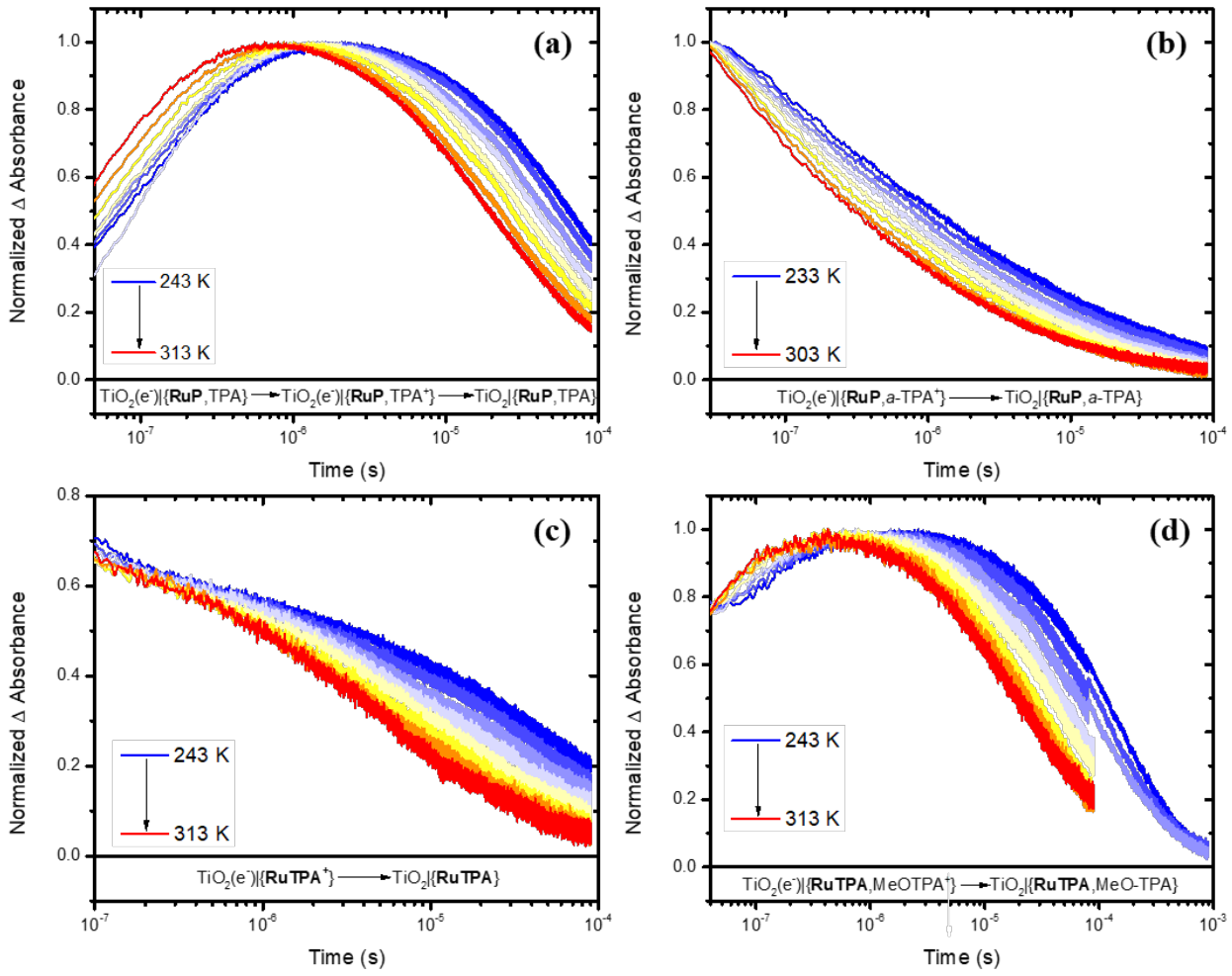

Figure 5. Single wavelength absorption changes measured after pulsed 532 nm laser excitation of TiO_2|{**RuP**,**Me**-TPA} (a), TiO_2|{**RuP**,***a*-TPA**} (b), TiO_2|{**RuTPA**} (c) and TiO_2|{**RuTPA**,**MeO**-TPA} (d) in 0.1M $LiClO_4$ CH_3CN electrolyte at various temperatures.

$$\ln k = \frac{-E_a}{R}\frac{1}{T} + \ln A \qquad (3)$$

$$\ln\frac{k}{T} = \frac{-\Delta H^{\ddagger}}{R}\frac{1}{T} + ln\frac{k_b}{h} + \frac{\Delta S^{\ddagger}}{R} \qquad (4)$$

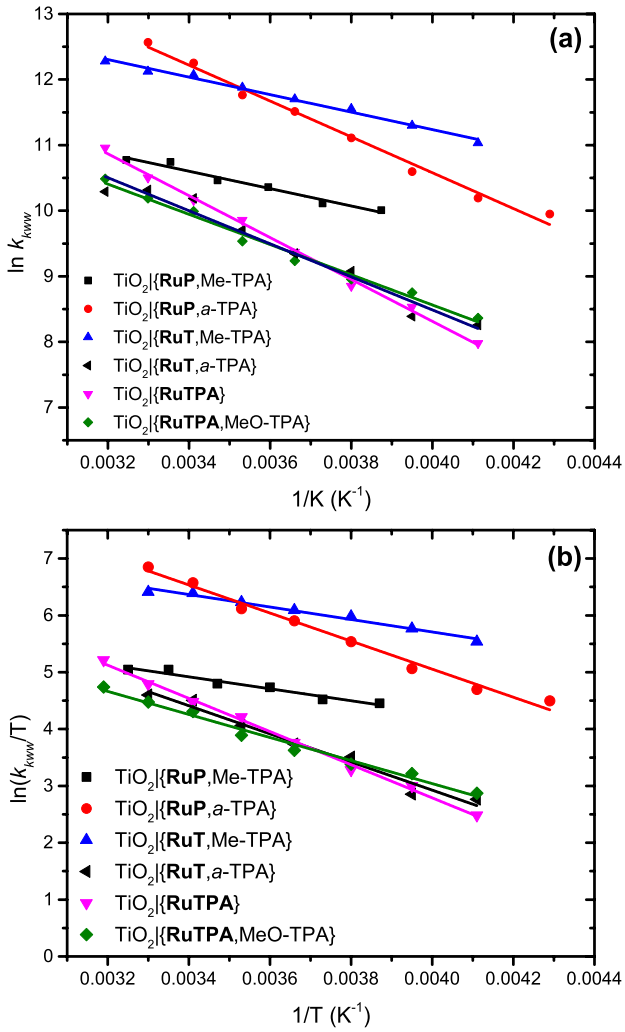

Figure 6. Arrhenius (a) and Eyring (b) analysis of charge recombination at the indicated dye-sensitized interfaces.

Table 2: Kinetic Rate Constants and Activation Energies for Recombination at Sensitized TiO_2 Interfaces.

Sensitized Interface	k_{kww} (x10^5 s^{-1}) [a]	ß [a]	ln(A)	Ea (kJ.mol^{-1})	Ea (eV)
TiO_2|{**RuP**,**Me**-TPA}	0.58 ± 0.03	0.7	15.1 ± 0.4	11 ± 1	0.11 ± 0.01
TiO_2|{**RuT**,**Me**-TPA}	0.82 ± 0.05	0.7	16.6 ± 0.2	11 ± 0.5	0.11 ± 0.01
TiO_2|{**RuP**,***a*-TPA**}	1.9 ± 0.1	0.17	21.5 ± 0.4	23 ± 1	0.24 ± 0.01
TiO_2|{**RuT**,***a*-TPA**}	1.6 ± 0.1	0.17	18.6 ± 0.7	21 ± 1.5	0.22 ± 0.02
TiO_2|{**RuTPA**}	1.3 ± 0.1	0.4	24.3 ± 0.9	27 ± 1	0.35 ± 0.02
TiO_2|{**RuTPA**,**MeO**-TPA}	0.69 ± 0.04	0.6	17.8 ± 0.4	19 ± 1	0.20 ± 0.01

[a]The room temperature average rate constant k_{kww} and the corresponding ß values were extracted from fits to the KWW function.

Table 3: The Activation Enthalpy ($\Delta H^{\ddagger}$), Entropy ($\Delta S^{\ddagger}$) and Gibbs Free Energy ($\Delta G^{\ddagger}$) for Recombination at Sensitized TiO_2 Interfaces.

Sensitized Interface	$\Delta H^{\ddagger}$ (kJ mol^{-1})	$\Delta S^{\ddagger}$ (J mol^{-1} K^{-1})	$\Delta G^{\ddagger}$ (kJ mol^{-1})
TiO_2|{**RuP**,**Me-TPA**}	9.1 ± 0.9	-127 ± 5	46.9
TiO_2|{**RuT**,**Me-TPA**}	8.8 ± 1.3	-118 ± 5	44.0
TiO_2|{**RuP**,***a*-TPA**}	20.5 ± 0.8	-73 ± 3	42.2
TiO_2|{**RuT**,***a*-TPA**}	20.6 ± 0.9	-84 ± 4	45.6
TiO_2|{**RuTPA**}	24.3 ± 0.8	-77 ± 3	47.2
TiO_2|{**RuTPA**,**MeO-TPA**}	16.8 ± 0.8	-104 ± 3	47.8

Discussion

In this report, pulsed light excitation of dye-sensitized mesoporous TiO_2 thin films resulted in rapid excited state electron injection, $k_{inj} > 10^8 s^{-1}$, followed by quantitative reduction of the oxidized dye sensitizer by TPA to yield the desired charge separated state comprised of an electron in TiO_2, $TiO_2(e^-)$, and TPA^+ whose subsequent recombination was the focus of this work. Related studies of electron transfer from photo-injected electrons in TiO_2 nanocrystallites ($TiO_2(e^-)$), to an electron acceptor (A) (**Equation 5**), has been the focus of prior publications where "A" was an oxidized dye[16, 30-33], halide[34-38], organic compound[20, 33, 39-41], transition metal complex[42-43], or water oxidation catalyst[5, 44-45].

$$TiO_2(e^-) + A \rightarrow TiO_2 + A^- \qquad (5)$$

This study complements, yet differs, from prior work by direct control of the acceptor in one of the following locations: 1) dissolved in the external CH_3CN solution that surrounds the mesoporous thin film; 2) anchored to the TiO_2 surface; or 3) covalently linked to the sensitizer. The utilization of a nearly identical series of TPA^+ acceptors afforded meaningful comparisons of the influence on the electron transfer kinetics and energetic barriers, which were indeed found to be acutely sensitive to the location of the TPA^+ in a sense that was not anticipated. For example, recombination to the **Me-**TPA^+ acceptors in fluid solution behaved like a first-order reaction while the surface anchored acceptor displayed behavior indicative of second-order recombination; behavior opposite to what might have been expected. Furthermore, the average recombination rate constant to the surface anchored ***a*-TPA$^+$** acceptor was 2-3 times larger, even though the measured activation barrier was about twice as large as that measured for the solution acceptor. Eyring analysis indicated a substantial entropic contribution to the large barrier for recombination. Below

these and other interesting behaviors are discussed in the context of prior literature with emphasis on the kinetics, activation barriers, and mechanism.

Kinetics. Excited-state injection in the electron accepting states in TiO_2 necessarily leads to the formation of one oxidizing equivalent (as an acceptor A) and one injected electron. Concentration is poorly defined at these interfaces and it is more precise to state that excited state injection yields equal numbers of injected electrons and electron acceptors. As a result, a second-order rate law might be expected (**Equation 6**) as is commonly observed for donors and acceptors in fluid solution.

$$\text{Rate} = k\,[\text{A}][\text{TiO}_2(e^-)] \qquad (\mathbf{6})$$

Indeed, early studies provided clear evidence for second-order recombination where A was an oxidized dye.[46-50] Compelling evidence for second-order recombination, gathered from laser irradiance studies, showed dramatically increased rates with increased numbers of acceptors and extracted rate constants that were concentration independent. Studies of other dye sensitized interfaces generally showed better fits to the stretched exponential or Kohlrausch-Williams-Watts (KWW) function $\Delta A = \Delta A e^{-(kt)^{ß}}$ indicative of dispersive kinetics.[20, 27, 30, 51-54] Here β is inversely related to a Lévy distribution of rate constants. When β = 1, a first-order reaction results, whereas smaller β values correspond to increasingly broad distributions of rate constants that have been recovered analytically or by approximation.[20,55] For charge recombination to oxidized sensitizers, β values less than 0.5 are typically reported.[56] However when dispersive kinetics were present, the transient kinetic data was sensitive to the initial number of injected electrons and decayed more quickly as the concentration increased.[30, 56-57] In other words, the laser irradiant dependent recombination dynamics could not be normalized like what would be expected for first-order recombination. These observations were important as they revealed how concentration studies (through excitation irradiance) could be used to determine reaction orders greater than one. They also indicated that when dispersive kinetics traces were identified, meaningful comparative studies required that the number of injected electrons be held constant. Interestingly, the dispersive nature of the recombination was initially attributed to transport of the injected electron back to the oxidized dye at the injection site; more recent data discussed below show that transport of the

oxidized dye across the nanocrystallite surface by intermolecular self-exchange, termed "hole-hopping", is also a key factor.[30, 57]

Highly relevant to the present study are experiments where the oxidized sensitizer is reduced by an electron donor, a reaction often called "sensitizer regeneration". Most prior literature on this subject has focused on iodide donors with remarkably slow interfacial electron transfer from $TiO_2(e^-)$ to I_3^- [34, 58] that was attributed to the unfavorable one-electron reduction potential of I_3^- ($E°(I_3^-/(I_2^{\bullet-},I^-)) = -0.58V$ vs SCE).[59] Other studies have focused on recombination to transition metal or organic based acceptors, often more amenable to systematic studies. [5, 45-47] For example, Hupp *et. al* found that recombination to a series of $Co(bpy')_3^{3+}$ acceptors was consistent with Marcus normal kinetic behavior.[60-62]

Herein, the location of the TPA had a significant influence on the recombination kinetics, with the fastest recombination occurring to surface anchored TPA, ***a*-TPA**. In this case, the β value was 0.17, which is similar to those previously reported for other surface anchored acceptors, including the oxidized sensitizers used herein.[12, 56, 63-64] The large average rate constant $1.7 \pm 0.2 \times 10^5\ s^{-1}$ is attributed to a rapid $TPA^{+/0}$ hole-hopping. Previous studies of a series of five *cis*-$Ru(dcb)(phen')(NCS)_2$, where phen' was a substituted 1,10-phenanthroline and dcb is 4,4'-$(CO_2H)_2$-2,2'-bipyridine, showed a direct correlation between hole-hopping and charge recombination. The sensitizers with the largest apparent diffusion coefficients for hole hopping showed the fastest recombination rates.[65] Furthermore, absorption anisotropy and variable surface coverage studies have shown that fast lateral hole-hopping consistently promotes faster charge recombination.[30] Hence, regeneration of the oxidized sensitizer by the surface anchored ***a*-TPA** resulted in a significant free energy loss (320 meV for **RuP** and 479 meV for **RuT**) and a shorter-lived injected electron, neither of which are desirable for solar applications.

A very recent study of dye regeneration by a series of triphenylamines revealed a first-order recombination mechanism,[20] consistent with a unimolecular-type reaction that provided the true electron transfer rate constant without complications from transport of the injected electron and/or oxidized dye. The electric field created by excited state injection was proposed to hold the TPA^+ proximate to the sensitized TiO_2 interface, inhibiting its ability to diffuse away from the interface. The electric fields generated by excited state injection are now known to be large, > 2 MV/cm,[19, 66] and there is a growing realization that such polarization restricts nuclear motion. First-order kinetics were only observed with those TPA derivatives that provided the largest driving force for

recombination. With TPA derivatives that were easily oxidized, dispersive kinetics were observed, which were irradiance dependent with $\beta = 0.7$. A reaction sphere model, similar to that of Perrin and Onsager, whose diameter increased with the free energy change was proposed. Recombination within the sphere was first-order while electrons outside had to undergo hopping, resulting in the observed dispersive kinetics.[20]

In this report, the **Me**-TPA donor yielded a β value of 0.7 which is much closer to first order-kinetics than that measured for the anchored TPA, ***a*-TPA**, where a β value of 0.17 was found to provide the best fit to the experimental data. Regarding **RuTPA**, a β value of 0.4 provided the best fit. This value is intermediate between **Me**-TPA and ***a*-TPA**, as is the average rate constant ($1.3 \pm 0.1 \times 10^5\ s^{-1}$). The significant difference in β values between the free and surface anchored TPA suggests that the two recombination events are subject to different degrees of electron diffusion, or are governed by a different process entirely. While **Me**-TPA can adopt several geometries on the surface of the metal oxide, ***a*-TPA** is restricted to a more orthogonal geometry. The former would allow for stronger coupling with the surface while the latter may promote rapid self-exchange reactions. This suggests that the overall electron recombination process is not solely dependent on diffusional process within the semiconductor, but rather is strongly influenced by the structure, geometry, configuration and dynamics of the electron acceptors.

Activated Interfacial Electron Transfer. This study also quantified the activation energy for recombination to the oxidized triphenylamines. The kinetics described above highlight that a major difficulty in interpretation rests on the nature of the rate determining step. This slow step may be electron $Ti^{IV/III}$ transport in the TiO_2, $TPA^{+/0}$ self-exchange across the surface, and/or the actual interfacial electron transfer reaction. A value for electron $Ti^{IV/III}$ transport in TiO_2 has been reported as 0.13 eV, which is about 12 ± 1 kJ.mol^{-1}.[67] This value is remarkably similar to that for Li^+ hops in $Li_{10}SnP_2S_{12}$-based composites,[68] and is hence consistent with ambipolar diffusion models that correlate electron transport with intercalated electrolyte cation motion.

The barrier for $TPA^{+/0}$ self-exchange is expected to be surface coverage dependent. It was previously shown with a series of $[Ru(LL)_2(dcb)]^{2+}$ complexes, where dcb is 4,4'-dicarboxy-2,2'-bipyridine and LL was either 4,4'-CF_3-, 4,4'-$(CH_3)_3C$- or 4,4'-CH_3-2,2'-bipyridine, that the activation energy for charge recombination were 22, 20 and 17 kJ mol^{-1}, respectively.[30] At sub-percolation coverages the activation energies were all around 22 kJ mol^{-1}. It should be stressed that charge recombination is also sensitive to the bridge orbitals that separate the acceptor from the

surface and specific bridge mediated pathways have been identified.[27] Finally, the anionic binding group (phosphonate or carboxylate) may also influence dynamics by precluding close encounters of the $TiO_2(e^-)$ with acceptors at the electrolyte interface.

The recombination activation energy to **Me**-TPA^+ and ***a*-TPA**$^+$ was 11 kJ.mol^{-1} and 21-23 kJ.mol^{-1}, respectively. Hence the barrier for the solution phase acceptor was very similar to that expected for $Ti^{IV/III}$ hopping alone, while that for the surface bound acceptor was in the same range as that previously reported for oxidized sensitizers.[30] The activation energy for recombination after excitation of TiO_2|{**RuTPA**} was determined to be 27 kJ.mol^{-1}, which was the largest barrier measured. The higher activation energy is related to the rigid molecular structure that fixes the TPA^+ further from the TiO_2 surface resulting in weaker electronic coupling as is described below. Interestingly, when the oxidizing equivalent was transferred from TiO_2|{**RuTPA**$^+$} to **MeO**-TPA in solution, the activation energy for recombination decreased to 19 kJ.mol^{-1}, but was still larger than that measured for **Me**-TPA^+ after light excitation of TiO_2|{**RuT**} or TiO_2|{**RuP**}. This behavior is attributed to **MeO**-TPA^+ being more weakly coupled to the TiO_2 surface than **Me**-TPA^+ as is discussed below.

An Eyring analysis of this same data was revealing.[69-72] The activation enthalpy ($\Delta H^‡$), entropy ($\Delta S^‡$) and Gibbs free energy ($\Delta G^‡$) are given in **Table 3**.[73] In fluid solution, the $\Delta H^‡$ value is related to E_a through **Equation 7** and good agreement was indeed found between the Arrhenius and the Eyring analysis.

$$\Delta H^‡ = \quad E_a - RT \quad (7)$$

The $\Delta S^‡$ values were consistently more negative with **Me-**TPA^+ present in the external solution compared to the surface anchored or ruthenium linked cases. For a first-order unimolecular reaction, $\Delta S^‡$ determines whether the reaction proceeds faster or slower. [69] Since previously reported recombination to solvated TPA'$^+$ derivatives displayed first-order kinetics that reflect the true interfacial electron transfer reaction, this data was reanalyzed with transition state theory and is given in **Table 4**.

Table 4: Electrochemical properties of four triphenylamine derivatives as well as the activation Enthalpy ($\Delta H^{\ddagger}$), Entropy ($\Delta S^{\ddagger}$), Gibbs Free Energy ($\Delta G^{\ddagger}$) for recombination at Sensitized TiO_2 Interfaces.

	$TPA^{+/0}$ (V vs. NHE)[a]	$\Delta H^{\ddagger}$ (kJ mol^{-1})	$\Delta S^{\ddagger}$ (J mol^{-1} K^{-1})	$\Delta G^{\ddagger}$ (kJ mol^{-1})
MeO-TPA	0.72 ± 0.01	10.8 ± 0.5	-127 ± 2	48.8
Me-TPA	0.93 ± 0.01	10.8 ± 0.5	-117 ± 2	45.7
Cl-TPA	1.24 ± 0.01	10.8 ± 0.5	-107 ± 2	42.9
Br-TPA	1.25 ± 0.01	10.8 ± 0.5	-103 ± 2	41.6

[a] Taken from ref[20]

Note that the values for **Me**-TPA^+ differ slightly from those in **Table 3** as a different sensitizer was utilized. In all cases the magnitude of $\Delta S^{\ddagger}$ was large and negative, - 115 ± 15 J $mol^{-1}K^{-1}$. An unfavorable activation entropy would be expected when an electron in a ~ 20 nm anatase TiO_2 nanocrystallite localizes on a surface absorbed TPA^+. The same expectation would hold for the surface anchored and sensitizer linked TPA^+ where the less negative $\Delta S^{\ddagger}$ = - 78 ± 6 J $mol^{-1}K^{-1}$, implies a less well-ordered transition state that may be influenced by the anionic surface anchoring groups. This allows one to rationalize why recombination to the surface anchored ***a*-TPA$^+$** was fast even though the barrier was large, the $\Delta S^{\ddagger}$ value was more favorable presumably because ***a*-TPA$^{+/0}$** self-exchange enabled less structural ordering in the transition state.

Interestingly, the $\Delta H^{\ddagger}$ and $\Delta S^{\ddagger}$ values in **Table 3** trade off on each other, such that the $\Delta G^{\ddagger}$ values were approximately the same and independent of the location of the TPA^+, 45 ± 3 kJ mol^{-1}. Such behavior is consistent with Marcus theory for non-adiabatic electron transfer and the expectation that ΔG^o was approximately constant for this study. For the prior work given in **Table 4**, ΔG^o was intentionally varied. The $\Delta G^{\ddagger}$ values decrease as the driving force increased, consistent with electron transfer in the normal kinetic region.

Conclusion

The data provides the first transition state analysis for interfacial electron transfer from $TiO_2(e^-)$ to **TPA$^+$** located at specific sites near the interface. Variable concentration studies revealed that recombination to **Me**-TPA^+ that had been dissolved in solution followed first-order kinetics while recombination to the surface anchored ***a*-TPA$^+$** showed evidence for higher order reactivity. Interestingly, recombination to ***a*-TPA$^+$** was faster than to **Me**-TPA^+ despite a higher

activation energy for the former. The origin of this behavior was traced to a less negative entropy of activation ($\Delta S^{\ddagger}$). Indeed, all Eyring analysis point toward unfavorable $\Delta S^{\ddagger}$ values as a key contributor to the barrier that results in the slow recombination kinetics commonly reported at dye-sensitized TiO_2 interfaces. Such behavior might be anticipated when an electron in an anatase TiO_2 nanocrystallite localizes on a molecular acceptor. The largest barrier was measured for $\mathbf{TPA}^{+}$ covalently linked to a ruthenium sensitizer that would be most practically useful for water splitting and photocatalysis applications where recombination is highly deleterious. Taken together, the results indicate that unfavorable entropy changes provide a large barrier that underlie the slow recombination at dye-sensitized interfaces yet the details of the transition state, and specifically the location of the acceptor, are important parameters for optimization.

Experimental

Materials:

NMR solvents were purchased from Cambridge Isotope Laboratories, Inc. and were used as received. Sephadex-LH20 used for column purification was purchased from GE Healthcare and was swelled in the eluent of choice overnight prior to use. All other reagents and solvents were obtained from commercial sources and used without further purification. Mesoporous thin films of anatase TiO_2 nanocrystallites were prepared according to previously reported literature, and either used immediately after preparation or were stored in an ~70°C oven until use. $[Ru(ttt)Cl_3]$[74] $[Ru(PO_3Et_2\text{-}C_6H_4\text{-}tpy)Cl_3]$[75] and 4,4'-bis-(diethylphosphonate)-2,2'-bipyridine[76] were prepared according to published procedures.

Sensitized TiO_2 thin films preparation:

Mesoporous nanocrystalline TiO_2 films were prepared using previously reported methods,[77] and were sensitized to visible light by submersion in acetonitrile solutions containing **RuP, RuT or RuTPA** for a minimum of 12 h. The surface coverage was varied between saturation coverages and ~30 % of saturation coverages by varying the sensitizer solution concentration. When studying ***a*-TPA**, films prepared with ~30% sensitizer saturation coverages were subsequently submerged in concentrated ***a*-TPA** ethanol solutions for a minimum of 12 hours, and the cosensitized films are abbreviated as $TiO_2|\{$**RuP**,***a*-TPA**$\}$ and $TiO_2|\{$**RuT**,***a*-TPA**$\}$.

Molecular Characterization:

Characteristic NMR spectra were obtained at room temperature on a Bruker Avance III 400 or 600 MHz spectrometer. Solvent residual peaks were used as internal standards for ^{1}H and ^{13}C chemical shift referencing. All $^{31}P\{^{1}H\}$ NMR spectra were obtained on a Bruker Advance spectrometer at 162 MHz and recorded relative to H_3PO_4. Generated spectra were processed using the MNOVA software.

Mass spectrometry was performed with a hybrid LTQ FT (ICR 7T) (ThermoFisher) mass spectrometer. Samples were introduced via a micro-electrospray source at a flow rate of 3 μL/min. The software Xcalibur (ThermoFisher) was used to analyze the data. Each mass spectrum was averaged over 200 time domains. Electrospray source conditions were set as: spray voltage 4.7 kV, sheath gas (nitrogen) 3 arb, auxiliary gas (nitrogen) 0 arb, sweep gas (nitrogen) 0 arb, capillary temperature 275 ºC, capillary voltage 35 V and tube lens voltage 110 V. The mass range was set to 150-2000 m/z. All measurements were recorded at a resolution setting of 100,000. Solutions were analyzed at 0.1 mg/mL or less based on responsiveness to the ESI mechanism. Low-resolution mass spectrometry (linear ion trap) provided independent verification of molecular weight distributions.

Spectroscopy:

UV−vis absorption spectra were recorded on a Varian Cary 60 UV−vis spectrophotometer. The extinction coefficients were determined from dilution of stock solutions and represent averages of at least two independent measurements. Nanosecond transient absorption measurements were acquired on a setup published previously.[78] All solutions were sparged with argon for at least 30 minutes before transient absorption experiments.

Electrochemical measurements were performed on a BASi Epsilon potentiostat in a standard three-electrode cell in CH_3CN electrolytes employing a platinum disk working electrode and a platinum mesh as an auxiliary electrode. A non-aqueous silver/silver chloride pseudo-reference electrode (Pine) was calibrated using ferrocene.

Compound Synthesis:

[Ru(4,4'-bis-(diethylphosphonate)-2,2'-bipyridine)(η^6-C_6H_6)Cl]Cl: A 100 mL round bottom flask equipped with a stir bar was charged with $[Ru(\eta^6\text{-}C_6H_6)Cl]_2Cl_2$ (148 mg, 0.295 mmol), and 4,4'-bis-(diethylphosphonate)-2,2'-bipyridine (255 mg, 0.595 mmol). The flask was flushed with nitrogen and then dichloromethane (30 mL) was introduced via syringe. The resulting suspension was stirred for 12 h at room temperature. The solvent was removed by rotary

evaporation, and then 50 mL of diethyl ether was added to the yellow-brown residue. The solid precipitate was collected by suction filtration and then dried in vacuo affording 310 mg (78%) of the product as a yellowish brown solid. ^{1}H NMR (400 MHz, $CDCl_3$): δ 10.22 (brs, 2H), 8.47 (d, *J* = 12.0 Hz, 2H), 8.05 (dd, *J* = 12.0, 4.0 Hz, 2H), 6.44 (s, 6H), 4.24 (m, 8H), 1.37 (q, *J* = 8.0 Hz, 12H). ^{31}P NMR (162 MHz, $CDCl_3$): δ 10.69. HRMS (ESI) m/z: $[M]^+$ for $C_{24}H_{32}N_2O_6P_2ClRu$: 643.04676; Found: 643.04541.

[Ru(4,4'-bis-(diethylphosphonate)-2,2'-bipyridine)(4,4'-di-*tert*-butyl-2,2'-bypridine)$_2$]Cl$_2$: A 100 mL Teflon microwave vessel equipped with a stir bar was charged with **[**Ru(4,4'-bis-(diethylphosphonate)-2,2'-bipyridine)(η^6-C_6H_6)Cl]Cl (164 mg, 0.241 mmol), and 4,4'-di-*tert*-butyl-2,2'-bypridine (132 mg, 0.493 mmol). A 30 mL portion of 2:1 ethanol:water was added to the microwave vessel and the suspension was then sonicated for 10 minutes. The resulting suspension was stirred and heated to 160 °C in a microwave reactor over a 5 minute period, and then held at that temperature for 20 minutes. After the reaction cooled to room temperature, the orange solution was filtered through a 0.2 μm syringe filter, and then added to a 100 mL round bottom flask. The solvent was removed by rotary evaporation, and then the residue was dissolved in a minimum amount of methanol. The orange solution was loaded onto a column of Sephadex LH-20 and eluted with methanol. The fractions containing the product were combined and the solvent removed by rotary evaporation. The resulting compound was treated with diethyl ether and the solid was collected by suction filtration and then dried in vacuo affording 219 mg (80%) of the product as a orange-red solid. ^{1}H NMR (400 MHz, CD_3OD): δ 8.84 (d, *J* = 16.0 Hz, 2H), 8.71(brs, 4H), 7.80 (m, 2H), 7.67 (m, 6H), 7.53 (m, 4H), 3.96 (m, 4H, under integrates due to partial hydrolysis under microwave conditions), 1.45 (s, 18H), 1.44 (s, 18H), 1.24 (t, *J* = 16.0 Hz, 6H, under integrates due to partial hydrolysis under microwave conditions). ^{31}P NMR (162 MHz, CD_3OD): δ 7.09. Several hydrolyzed products were observed by HRMS; HRMS (ESI) m/z: $[M]^+$ for $C_{52}H_{69}N_6O_6P_2Ru$: 1037.37973; Found: 1037.38141; HRMS (ESI) m/z: $[2M]^{2+}$ for $C_{50}H_{65}N_6O_6P_2Ru$: 1009.34843; Found: 1009.35007

[Ru(4,4'-bis-(PO_3H_2)-2,2'-bipyridine)(4,4'-di-tert-butyl-2,2'-bypridine)$_2$](PF_6)$_2$ "RuP": A 50 mL round bottom flask was charged with Ru(4,4'- (ethyl hydrogen phosphonate)-2,2'-bipyridine)(4,4'-di-*tert*-butyl-2,2'-bypridine)$_2$]Cl_2 (237 mg, 0.208 mmol). The flask was sealed with a rubber septum, and flushed with nitrogen before the introduction of 20 mL of anhydrous CH_3CN. Finally, trimethylsilyl bromide (100 μL, 0.758 mmol) was added by syringe. The reaction

was heated to 70 ºC for 2 days. After cooling to room temperature, 1 mL of methanol was added to the orange solution. The solvent was removed in vacuo affording an orange-red residue. The residue was dissolved in a minimal amount of water, and the product was precipitated by the addition of saturated aqueous NH_4PF_6. The precipitate was collected and washed with a small amount of cold water, and then dried in vacuo affording 178 mg (69%). ^{1}H NMR (500 MHz, CD_3OD) δ 8.84 (d, *J* = 12.1 Hz, 2H), 8.72 (dd, *J* = 5.6, 2.0 Hz, 4H), 7.76 (d, *J* = 4.0 Hz, 2H), 7.67 (m, 6H), 7.52 (m, 4H), 1.45 (s, 18H), 1.44 (s, 18H). ^{31}P NMR (162 MHz, CD_3OD): δ 5.01. HRMS (ESI) m/z: $[M]^+$ for $C_{46}H_{57}N_6O_6P_2Ru$: 953.28583; Found: 953. 28687.

4-[N,N-di(*p*-tolyl)amino]benzylalcohol: The synthetic procedure was adapted from a previously published protocol.[79] 4-(N,N-di-*p*-tolylamino)benzaldehyde (1.38g, 4.58 mmol) was dissolved in 30 mL of ethanol. Sodium borohydride (675mg, 17.84 mmol) was then added and the reaction mixture was heated at reflux for 4 hours. Over time, the color changed from yellow to colorless. After reaction, the mixture was brought to room temperature and poured into 50 mL of water. The mixture was extracted three times with diethylether. The organic layers were combined, dried over anhydrous $MgSO_4$ and filtered. The filtrate was finally evaporated under reduced pressure to yield the title compound as a white powder (1.36 g, 98 %). ^{1}H NMR ($CDCl_3$, 600 MHz): δ 7.20 (2H, d, J = 8.5 Hz), 7.06 (4H, d, J = 8.2 Hz), 7.02 (2H, d, J = 8.4 Hz), 6.98 (4H, d, J = 8.4 Hz), 4.61 (2H, s), 2.31 (6H, s), 1.59 (1H, s). ^{13}C NMR ($CDCl_3$, 600 MHz): 148.04, 145.41, 134.04, 132.60, 129.99, 129.14, 128.33, 124.63, 124.56, 122.88, 65.33, 20.95. HRMS (ESI-MS) m/z: $[M\text{-}OH]^+$ Calcd for $C_{21}H_{20}N$ 286.15957; Found 286.15888; : $[M+H]^+$ Calcd for $C_{21}H_{21}NO$ 304.17014; Found 304.16851.

4-[N,N-di(*p*-tolyl)amino]benzylphosphonic ester: 4-(N,N-di(p-tolyl)amino)- benzylalcohol (1.04 g, 3.4 mmol) was dissolved in 13 mL of triethylphosphite. The mixture was cooled to 0°C and sparged with argon for 30 minutes. A 900 mg (3.5 mmol) portion of I_2 was then added, and the mixture is stirred at 0°C for 5 minutes before being brought to room temperature and stirred for an additional 12 hours. After this time had elapsed, the triethylphosphite was removed under vacuum and the residue was purified through column chromatography (SiO_2, CH_2Cl_2:MeOH 100:0 to 96:4). The final product was recovered as a yellow oil (1.16 g, 80%) ^{1}H NMR (600 MHz, $CDCl_3$): δ 7.13 (2H, dd, J = 8.6, 2.5 Hz), 7.04 (4H, d, J = 8.2 Hz), 6.97 (6H, m), 4.04 (4H, m), 3.09 (2H, d, J = 21.3 Hz), 2.30 (6H, s), 1.26 (6H, t, J = 7.2 Hz). ^{13}C NMR (600 MHz, $CDCl_3$): δ 147.14, 147.12, 145.38,

132.42, 130.53, 130.48, 129.91, 124.49, 124.41, 122.97, 122.95, 62.21, 62.16, 33.52, 32.61, 20.90, 16.53, 16.49. HRMS (ESI-MS) m/z: $[M]^{2+}$ Calcd for $C_{25}H_{30}NO_3P$ 424.20417; Found 424.20403.

4-[N,N-di(*p*-tolyl)amino]benzylphosphonic acid "*a*-TPA": 4-[N,N-di(p-tolyl)amino]benzyl-phosphonic ester (423 mg, 1 mmol) was dissolved in 3 mL of dry CH_3CN. The mixture was cooled to 0°C and TMSBr (460 mg, 396 µL, 3 mmol) was added. The mixture was then stirred overnight at room temperature. After this reaction completed, the solvent was removed by vacuum distillation and 5 mL of methanol was added to the resulting solid. Aqueous sodium hydroxide was added until the solution reached pH~8, which was followed by the formation of a white precipitate that was collected by filtration. The solid was then dissolved in 10 mL of water and precipitated by the addition of 0.1 M HCl. The off-white solid was filtered, washed with water and dried under vacuum (340 mg, 93 %). ^{1}H NMR (600 MHz, CD_3OD): δ 7.16 (2H, d, J = 7.6 Hz), 7.04 (4H, d, J = 8.2 Hz), 6.88 (4H, m), 3.01 (2H, d, J = 21.1Hz), 2.28 (6H, s). ^{13}C NMR (600 MHz, CD_3OD): δ 148.03, 146.92, 133.36, 131.63, 131.59, 130.77, 125.25, 124.20, 35.82 20.82. HRMS (ESI-MS) m/z: $[M+H]^+$ Calcd for $C_{21}H_{22}NO_3P$ 368.14157; Found 368.14135. $[M]^+$ Calcd for $C_{21}H_{22}NO_3P$ 367.13374; Found 368.14135.

$[Ru(ttt)(tpy\text{-}C_6H_4\text{-}PO_3Et_2)]^{2+}.2PF_6$. (Ru-$PO_3Et_2$). $[Ru(ttt)Cl_3]$ (156 mg, 0.256 mmol) and tpy-C_6H_4-PO_3Et_2 (114 mg, 0.256 mmol) were place in a microwave tube. Ethanol (18 mL) and N-ethylmorpholine (1.5 mL) were added. The microwave tube was then sealed and heated under microwave irradiation at 120°C for 2 hours. After reaction, 10 mL of water and 2 mL of a saturated NH_4PF_6 aqueous solution were added. The ethanol was removed under reduced pressure and the resulting solid was recovered by filtration and washed with water, small amounts of ethanol, and diethylether. The product was obtained as a red powder (280 mg, 88%).

^{1}H NMR (400 MHz, CD_3CN): δ 9.00 (s, 2H), 8.78 (s, 2H), 8.64 (d, *J* = 8.1 Hz, 2H), 8.51 (d, *J* = 2.0 Hz, 2H), 8.36 – 8.27 (m, 2H), 8.12 (dd, *J* = 12.8, 8.3 Hz, 2H), 7.95 (td, *J* = 7.8, 1.5 Hz, 2H), 7.36 (d, *J* = 5.0 Hz, 2H), 7.28 – 7.17 (m, 4H), 7.12 (dd, *J* = 6.0, 2.1 Hz, 2H), 4.19 (ddd, *J* = 8.2, 7.1, 2.8 Hz, 4H), 1.75 (s, 9H), 1.38 (d, *J* = 7.0 Hz, 6H), 1.31 (s, 18H). HRMS (ESI-MS) m/z: $[M-PF_6]^+$ Calcd for $C_{52}H_{59}F_6N_6O_3P_2Ru$ 1093.3071; Found 1093.3017.

$[Ru(ttt)(tpy\text{-}C_6H_4\text{-}PO_3H_2)]^{2+}.2PF_6$ "RuT". $[Ru(ttt)(tpy\text{-}C_6H_4\text{-}PO_3Et_2)]^{2+}.2PF_6$ (330 mg, 0.266 mmol) was dissolved in 25 mL of CH_3CN. Trimethylsilylbromide TMSBr (180 µL, 1.34 mmol) was added and the mixture was stirred at 70°C under an argon atmosphere for 24 hours. After reaction, the mixture was brought to room temperature and 5 mL of methanol was added.

The resulting solution was stirred for 30 minutes and evaporated to dryness under reduced pressure. The residue was washed with small amounts of cold CH_3CN and diethylether to obtain the title compound as a red powder (297 mg, 94 %).

^{1}H NMR (400 MHz, CD_3OD): δ 9.31 (s, 2H), 9.08 (s, 2H), 8.90 (d, *J* = 8.1 Hz, 2H), 8.79 (d, *J* = 2.0 Hz, 2H), 8.42 (dd, *J* = 8.0, 3.1 Hz, 2H), 8.16 (dd, *J* = 13.1, 8.0 Hz, 2H), 8.01 (td, *J* = 7.9, 1.5 Hz, 2H), 7.50 – 7.42 (m, 2H), 7.37 (d, *J* = 6.0 Hz, 2H), 7.32 – 7.22 (m, 4H), 1.81 (s, 9H), 1.35 (s, 18H). HRMS (ESI-MS) m/z: $[M-(PF_6)_2]^{2+}$ Calcd for $C_{48}H_{51}N_6O_3P_1Ru$ 446.1402; Found 446.1389.

4''-(4,4'-dimethyl-triphenylamine)-terpyridine (tpy-TPA): 4-(di-*p*-tolylamino)benzaldehyde (1g, 3.66 mmol) and 2-acetylpyridine (752 µL, 6.70 mmol) are placed in 17 mL of absolute ethanol. The mixture is stirred and KOH (520 mg, 9.27 mmol) as well as ammonium hydroxide (28%, 9.7 mL) are added. The reaction mixture is stirred at room temperature for 24 hours. After reaction, the mixture is filtered, washed with cold ethanol and diethyl ether. The product is finally obtained as a yellow powder (1.3 g, 72 %).

^{1}H NMR (400 MHz, $CDCl_3$): δ 8.78 – 8.71 (m, 4H), 8.68 (d, *J* = 8.0 Hz, 2H), 7.90 (td, *J* = 7.7, 1.8 Hz, 2H), 7.78 (d, *J* = 8.7 Hz, 2H), 7.36 (ddd, *J* = 7.6, 4.8, 1.2 Hz, 2H), 7.11 (dd, *J* = 8.6, 2.5 Hz, 6H), 7.05 (d, *J* = 8.5 Hz, 4H), 2.34 (s, 6H). HRMS (ESI-MS) m/z: $[M+H]^+$ Calcd for $C_{35}H_{29}N_4$ 505.23922; Found 505.23842.

$[Ru(tpy\text{-}C_6H_4\text{-}PO_3Et_2)(tpy\text{-}TPA)]^{2+}.2PF_6$. $[Ru(PO_3Et_2\text{-}C_6H_4\text{-}tpy)Cl_3]$ (130 mg, 0.2 mmol) and 4'-(4,4'-dimethyl-triphenylamine)-terpyridine (tpy-TPA) (106 mg, 0.21 mmol) were place in a microwave tube. Ethanol (14 mL) and N-ethylmorpholine (1.2 mL) were added. The microwave tube was then sealed and heated under microwave irradiation at 120°C for 2 hours. After reaction, 10 mL of water and 2 mL of a saturated NH_4PF_6 aqueous solution were added. The ethanol was removed under reduced pressure. The mixture was then centrifuged and the precipitate was washed with water. This procedure was repeated twice. The solid was then dried under vacuum to give the title compound as a red powder (240 mg, 89%).

^{1}H NMR (400 MHz, CD_3CN): δ 9.03 (d, *J* = 6.1 Hz, 2H), 8.93 (d, *J* = 5.8 Hz, 2H), 8.63 (dd, *J* = 10.3, 8.2 Hz, 4H), 8.32 (dd, *J* = 8.3, 3.5 Hz, 2H), 8.13 (dd, *J* = 12.8, 8.2 Hz, 2H), 8.07 (d, *J* = 8.8 Hz, 2H), 7.98 – 7.90 (m, 4H), 7.46 (d, *J* = 5.6 Hz, 2H), 7.40 (d, *J* = 5.9 Hz, 2H), 7.25 (d, *J* = 8.1 Hz, 4H), 7.22 – 7.12 (m, 10H), 4.19 (tdq, *J* = 10.2, 6.0, 3.1 Hz, 4H), 2.37 (s, 6H), 1.37 (t, *J* = 7.0 Hz, 6H). HRMS (ESI-MS) m/z: $[M]^+$ Calcd for $C_{60}H_{52}N_7O_3P2F_6Ru$: 1196.25545; Found 1196.26098

[Ru(tpy-C_6H_4-PO_3H_2)(tpy-TPA)]$^{2+}$ "RuTPA". [Ru(tpy-C_6H_4-PO_3Et_2)(tpy-TPA)]$^{2+}$.2PF_6 (60 mg, 0.045 mmol) was dissolved in 5 mL of acetonitrile. Trimethylsilyl bromide TMSBr (18 µL, 0.134 mmol) was added and the mixture was stirred at 70°C under an argon atmosphere for 24 hours. After reaction, the mixture was brought to room temperature and 1 mL of methanol was added. The resulting solution was stirred for 30 minutes and evaporated to dryness under reduced pressure. The residue was washed with small amounts of cold acetonitrile and diethylether to obtain the title compound as a red powder (45 mg, 87 %).

^{1}H NMR (400 MHz, CD_3CN): δ 9.06 (s, 2H), 8.93 (d, *J* = 6.1 Hz, 2H), 8.74 – 8.54 (m, 4H), 8.24 (d, *J* = 47.1 Hz, 4H), 8.06 (dd, *J* = 8.8, 3.2 Hz, 2H), 8.00 – 7.80 (m, 4H), 7.43 (dd, *J* = 16.1, 5.6 Hz, 4H), 7.25 (d, *J* = 8.0 Hz, 4H), 7.16 (dd, *J* = 15.7, 8.1 Hz, 10H), 2.38 (s, 6H). HRMS (ESI-MS) m/z: [M]$^{2+}$ Calcd for $C_{56}H_{44}N_7O_3P_1Ru$ 497.61433 (1031.2478); Found 497.61565.

Associated Content

Supporting Information: Absorption spectra, cyclic voltammograms, oxidative spectroelectrochemistry measurements, Single wavelength absorption changes of TiO_2|{**RuT**}, ^{1}H and ^{13}C NMR spectra on newly reported compounds. This material is available free of charge on the ACS Publications website.

Author Information.

Corresponding Author

gjmeyer@email.unc.edu

Acknowledgments.

This material is based upon work solely supported as part of the UNC EFRC: Center for Solar Fuels, an Energy Frontier Research Center funded by the U.S. Department of Energy, Office of Science, Office of Basic Energy Sciences under Award Number DE-SC0001011. L. T.-G. acknowledges personal fellowships from the Belgian American Educational Foundation (BAEF) as well as the Bourse d'Excellence Wallonie-Bruxelles (WBI.World). The authors would like to thank Matthew D. Brady for help in spectroelectrochemical measurements as well as the University of North Carolina Department of Chemistry Mass Spectrometry Core Laboratory and Dr. B. Ehrmann for assistance with mass spectrometry analysis.

References

1. Alibabaei, L.; Brennaman, M. K.; Meyer, T. J., Light-Driven Water Splitting in the Dye-Sensitized Photoelectrosynthesis Cell. In *Molecular Devices for Solar Energy Conversion and Storage*, Tian, H.; Boschloo, G.; Hagfeldt, A., Eds. Springer Singapore: Singapore, 2018; pp 229-257.
2. Ardo, S.; Meyer, G. J. *Chem. Soc. Rev.* **2009,** *38*, 115-164.
3. Berardi, S.; Cristino, V.; Canton, M.; Boaretto, R.; Argazzi, R.; Benazzi, E.; Ganzer, L.; Borrego Varillas, R.; Cerullo, G.; Syrgiannis, Z.; Rigodanza, F.; Prato, M.; Bignozzi, C. A.; Caramori, S. *J. Phys. Chem. C* **2017,** *121*, 17737-17745.
4. Brady, M. D.; Sampaio, R. N.; Wang, D.; Meyer, T. J.; Meyer, G. J. *J. Am. Chem. Soc.* **2017,** *139*, 15612-15615.
5. Brennaman, M. K.; Dillon, R. J.; Alibabaei, L.; Gish, M. K.; Dares, C. J.; Ashford, D. L.; House, R. L.; Meyer, G. J.; Papanikolas, J. M.; Meyer, T. J. *J. Am. Chem. Soc.* **2016,** *138*, 13085-13102.
6. McDaniel, N. D.; Bernhard, S. *Dalton Trans.* **2010,** *39*, 10021-10030.
7. O'Regan, B.; Grätzel, M. *Nature* **1991,** *353*, 737.
8. Vlachopoulos, N.; Liska, P.; Augustynski, J.; Graetzel, M. *J. Am. Chem. Soc.* **1988,** *110*, 1216-1220.
9. Zhang, J.; Freitag, M.; Hagfeldt, A.; Boschloo, G., Solid-State Dye-Sensitized Solar Cells. In *Molecular Devices for Solar Energy Conversion and Storage*, Tian, H.; Boschloo, G.; Hagfeldt, A., Eds. Springer Singapore: Singapore, 2018; pp 151-185.
10. Tian, H.; Kloo, L., Liquid Dye-Sensitized Solar Cells. In *Molecular Devices for Solar Energy Conversion and Storage*, Tian, H.; Boschloo, G.; Hagfeldt, A., Eds. Springer Singapore: Singapore, 2018; pp 109-149.
11. Listorti, A.; O'Regan, B.; Durrant, J. R. *Chem. Mater.* **2011,** *23*, 3381-3399.
12. Robson, K. C. D.; Hu, K.; Meyer, G. J.; Berlinguette, C. P. *J. Am. Chem. Soc.* **2013,** *135*, 1961-1971.
13. Alibabaei, L.; Brennaman, M. K.; Norris, M. R.; Kalanyan, B.; Song, W.; Losego, M. D.; Concepcion, J. J.; Binstead, R. A.; Parsons, G. N.; Meyer, T. J. *P. Natl. Acad. Sci. USA* **2013,** *110*, 20008-20013.
14. Alibabaei, L.; Farnum, B. H.; Kalanyan, B.; Brennaman, M. K.; Losego, M. D.; Parsons, G. N.; Meyer, T. J. *Nano Lett.* **2014,** *14*, 3255-3261.
15. Eberhart, M. S.; Wang, D.; Sampaio, R. N.; Marquard, S. L.; Shan, B.; Brennaman, M. K.; Meyer, G. J.; Dares, C.; Meyer, T. J. *J. Am. Chem. Soc.* **2017,** *139*, 16248-16255.
16. Knauf, R. R.; Kalanyan, B.; Parsons, G. N.; Dempsey, J. L. *J. Phys. Chem. C* **2015,** *119*, 28353-28360.
17. Sherman, B. D.; Ashford, D. L.; Lapides, A. M.; Sheridan, M. V.; Wee, K.-R.; Meyer, T. J. *J. Phys. Chem. Lett.* **2015,** *6*, 3213-3217.
18. Wee, K.-R.; Sherman, B. D.; Brennaman, M. K.; Sheridan, M. V.; Nayak, A.; Alibabaei, L.; Meyer, T. J. *J. Mater. Chem. A* **2016,** *4*, 2969-2975.
19. DiMarco, B. N.; O'Donnell, R. M.; Meyer, G. J. *J. Phys. Chem. C* **2015,** *119*, 21599-21604.
20. DiMarco, B. N.; Troian-Gautier, L.; Neiva Sampaio, R.; Meyer, G. J. *Chem. Sci.* **2018,** *9*, 940-949.
21. Cazzanti, S.; Caramori, S.; Argazzi, R.; Elliott, C. M.; Bignozzi, C. A. *J. Am. Chem. Soc.* **2006,** *128*, 9996-9997.
22. Hao, Y.; Yang, W.; Zhang, L.; Jiang, R.; Mijangos, E.; Saygili, Y.; Hammarström, L.; Hagfeldt, A.; Boschloo, G. *Nature Comm.* **2016,** *7*, 13934.
23. Planells, M.; Abate, A.; Hollman, D. J.; Stranks, S. D.; Bharti, V.; Gaur, J.; Mohanty, D.; Chand, S.; Snaith, H. J.; Robertson, N. *J. Mater. Chem. A* **2013,** *1*, 6949-6960.
24. Ardo, S.; Sun, Y.; Staniszewski, A.; Castellano, F. N.; Meyer, G. J. *J. Am. Chem. Soc.* **2010,** *132*, 6696-6709.
25. Cappel, U. B.; Feldt, S. M.; Schöneboom, J.; Hagfeldt, A.; Boschloo, G. *J. Am. Chem. Soc.* **2010,** *132*, 9096-9101.
26. O'Donnell, R. M.; Sampaio, R. N.; Barr, T. J.; Meyer, G. J. *J. Phys. Chem. C* **2014,** *118*, 16976-16986.

27. Hu, K.; Blair, A. D.; Piechota, E. J.; Schauer, P. A.; Sampaio, R. N.; Parlane, F. G. L.; Meyer, G. J.; Berlinguette, C. P. *Nature Chem.* **2016,** *8*, 853.
28. Scher, H.; Montroll, E. W. *Phys. Rev. B* **1975,** *12*, 2455-2477.
29. Williams, G.; Watts, D. C. *T. Faraday Soc.* **1970,** *66*, 80-85.
30. Sampaio, R. N.; DiMarco, B. N.; Meyer, G. J. *ACS Energy Lett.* **2017,** *2*, 2402-2407.
31. Ward, C. L.; O'Donnell, R. M.; DiMarco, B. N.; Meyer, G. J. *J. Phys. Chem. C* **2015,** *119*, 25273-25281.
32. Argazzi, R.; Bignozzi, C. A.; Heimer, T. A.; Castellano, F. N.; Meyer, G. J. *J. Phys. Chem. B* **1997,** *101*, 2591-2597.
33. Bonhôte, P.; Moser, J.-E.; Humphry-Baker, R.; Vlachopoulos, N.; Zakeeruddin, S. M.; Walder, L.; Grätzel, M. *J. Am. Chem. Soc.* **1999,** *121*, 1324-1336.
34. Rowley, J. G.; Farnum, B. H.; Ardo, S.; Meyer, G. J. *J. Phys. Chem. Lett.* **2010,** *1*, 3132-3140.
35. Hu, K.; Severin, H. A.; Koivisto, B. D.; Robson, K. C. D.; Schott, E.; Arratia-Perez, R.; Meyer, G. J.; Berlinguette, C. P. *J. Phys. Chem. C* **2014,** *118*, 17079-17089.
36. Staniszewski, A.; Ardo, S.; Sun, Y.; Castellano, F. N.; Meyer, G. J. *J. Am. Chem. Soc.* **2008,** *130*, 11586-11587.
37. Gregg, B. A.; Pichot, F.; Ferrere, S.; Fields, C. L. *J. Phys. Chem. B* **2001,** *105*, 1422-1429.
38. Durrant, J. R. *J. Photoch. Photobio. A* **2002,** *148*, 5-10.
39. Hu, K.; Robson, K. C. D.; Berlinguette, C. P.; Meyer, G. J. *Thin Solid Films* **2014,** *560*, 49-54.
40. Haque, S. A.; Handa, S.; Peter, K.; Palomares, E.; Thelakkat, M.; Durrant, J. R. *Angew. Chem. Int. Ed.* **2005,** *44*, 5740-5744.
41. Hirata, N.; Lagref, J.-J.; Palomares, E. J.; Durrant, J. R.; Nazeeruddin, M. K.; Gratzel, M.; Di Censo, D. *Chem. Eur. J.* **2004,** *10*, 595-602.
42. Nusbaumer, H.; Moser, J.-E.; Zakeeruddin, S. M.; Nazeeruddin, M. K.; Grätzel, M. *J. Phys. Chem. B* **2001,** *105*, 10461-10464.
43. Kleverlaan, C.; Alebbi, M.; Argazzi, R.; Bignozzi, C. A.; Hasselmann, G. M.; Meyer, G. J. *Inorg. Chem.* **2000,** *39*, 1342-1343.
44. Song, W.; Ito, A.; Binstead, R. A.; Hanson, K.; Luo, H.; Brennaman, M. K.; Concepcion, J. J.; Meyer, T. J. *J. Am. Chem. Soc.* **2013,** *135*, 11587-11594.
45. Hu, K.; Sampaio, R. N.; Marquard, S. L.; Brennaman, M. K.; Tamaki, Y.; Meyer, T. J.; Meyer, G. J. *Inorg. Chem.* **2018**, *57*, 486-494.
46. Kelly, C. A.; Farzad, F.; Thompson, D. W.; Meyer, G. J. *Langmuir* **1999,** *15*, 731-737.
47. Kelly, C. A.; Farzad, F.; Thompson, D. W.; Stipkala, J. M.; Meyer, G. J. *Langmuir* **1999,** *15*, 7047-7054.
48. Kilså, K.; Mayo, E. I.; Kuciauskas, D.; Villahermosa, R.; Lewis, N. S.; Winkler, J. R.; Gray, H. B. *J. Phys. Chem. A* **2003,** *107*, 3379-3383.
49. Kuciauskas, D.; Freund, M. S.; Gray, H. B.; Winkler, J. R.; Lewis, N. S. *J. Phys. Chem. B* **2001,** *105*, 392-403.
50. Thompson, D. W.; Kelly, C. A.; Farzad, F.; Meyer, G. J. *Langmuir* **1999,** *15*, 650-653.
51. Brennan, B. J.; Regan, K. P.; Durrell, A. C.; Schmuttenmaer, C. A.; Brudvig, G. W. *ACS Energy Lett.* **2017,** *2*, 168-173.
52. Green, A. N. M.; Palomares, E.; Haque, S. A.; Kroon, J. M.; Durrant, J. R. *J. Phys. Chem. B* **2005,** *109*, 12525-12533.
53. Saavedra Becerril, V.; Sundin, E.; Mapar, M.; Abrahamsson, M. *Phys. Chem. Chem. Phys.* **2017,** *19*, 22684-22690.
54. Yang, W.; Vlachopoulos, N.; Boschloo, G. *ACS Energy Lett.* **2017,** *2*, 161-167.
55. Heimer, T. A.; Meyer, G. J. *Journal of Luminescence* **1996,** *70*, 468-478.
56. Brigham, E. C.; Meyer, G. J. *J. Phys. Chem. C* **2014,** *118*, 7886-7893.
57. Clifford, J. N.; Palomares, E.; Nazeeruddin, M. K.; Grätzel, M.; Nelson, J.; Li, X.; Long, N. J.; Durrant, J. R. *J. Am. Chem. Soc.* **2004,** *126*, 5225-5233.

58. Rowley, J. G.; Ardo, S.; Sun, Y.; Castellano, F. N.; Meyer, G. J. *J. Phys. Chem. C* **2011,** *115*, 20316-20325.
59. Farnum, B. H.; Gardner, J. M.; Meyer, G. J. *Inorg. Chem.* **2010,** *49*, 10223-10225.
60. DeVries, M. J.; Pellin, M. J.; Hupp, J. T. *Langmuir* **2010,** *26*, 9082-9087.
61. Hamann, T. W.; Farha, O. K.; Hupp, J. T. *J. Phys. Chem. C* **2008,** *112*, 19756-19764.
62. Ondersma, J. W.; Hamann, T. W. *J. Am. Chem. Soc.* **2011,** *133*, 8264-8271.
63. Hu, K.; Robson, K. C. D.; Beauvilliers, E. E.; Schott, E.; Zarate, X.; Arratia-Perez, R.; Berlinguette, C. P.; Meyer, G. J. *J. Am. Chem. Soc.* **2014,** *136*, 1034-1046.
64. Hu, K.; Robson, K. C. D.; Johansson, P. G.; Berlinguette, C. P.; Meyer, G. J. *J. Am. Chem. Soc.* **2012,** *134*, 8352-8355.
65. Sampaio, R. N.; Müller, A. V.; Polo, A. S.; Meyer, G. J. *ACS Appl. Mater. Inter.* **2017,** *9*, 33446-33454.
66. Farnum, B. H.; Morseth, Z. A.; Brennaman, M. K.; Papanikolas, J. M.; Meyer, T. J. *J. Am. Chem. Soc.* **2014,** *136*, 15869-15872.
67. Boschloo, G.; Hagfeldt, A. *J. Phys. Chem. B* **2005,** *109*, 12093-12098.
68. Kaus, M.; Stöffler, H.; Yavuz, M.; Zinkevich, T.; Knapp, M.; Ehrenberg, H.; Indris, S. *J. Phys. Chem. C* **2017,** *121*, 23370-23376.
69. Frost, A. A.; Pearson, n. R. G., *Kinetics and Mechanism - A study of Homogeneous Chemical Reactions*. John Wiler & Sons, Inc, Hoboken, NJ, 1961.
70. Atkins, P.; De Paula, J., *Physical Chemistry*. Oxford University Press: 2010.
71. Eyring, H. *J. Chem. Phys.* **1935,** *3*, 107-115.
72. Eyring, H. *Chem. Rev.* **1935,** *17*, 65-77.
73. Saracini, C.; Ohkubo, K.; Suenobu, T.; Meyer, G. J.; Karlin, K. D.; Fukuzumi, S. *J. Am. Chem. Soc.* **2015,** *137*, 15865-15874.
74. Hadda, T. B.; Le Bozec, H. *Polyhedron* **1988,** *7*, 575-577.
75. Lanzilotto, A.; Buldt, L. A.; Schmidt, H. C.; Prescimone, A.; Wenger, O. S.; Constable, E. C.; Housecroft, C. E. *RSC Adv.* **2016,** *6*, 15370-15381.
76. Norris, M. R.; Concepcion, J. J.; Glasson, C. R. K.; Fang, Z.; Lapides, A. M.; Ashford, D. L.; Templeton, J. L.; Meyer, T. J. *Inorg. Chem.* **2013,** *52*, 12492-12501.
77. Heimer, T. A.; D'Arcangelis, S. T.; Farzad, F.; Stipkala, J. M.; Meyer, G. J. *Inorg. Chem.* **1996,** *35*, 5319-5324.
78. Argazzi, R.; Bignozzi, C. A.; Heimer, T. A.; Castellano, F. N.; Meyer, G. J. *Inorg. Chem.* **1994,** *33*, 5741-5749.
79. Zhou, X.; Li, X.; Liu, Y.; Li, R.; Jiang, K.; Xia, J. *Org. Electron.* **2015,** *25*, 245-253.

For Table of Contents Only